J|A|C|S
ARTICLES
Published on Web 03/31/2007

Nickel-Specific Response in the Transcriptional Regulator, *Escherichia coli* NikR

Sharon Leitch,[†] Michael J. Bradley,[‡] Jessica L. Rowe,[‡] Peter T. Chivers,[‡] and Michael J. Maroney*,[†]

Contribution from the Department of Chemistry, University of Massachusetts, Amherst, Massachusetts 01003, and Department of Biochemistry and Molecular Biophysics, Washington University School of Medicine, Saint Louis, Missouri 63110

Received November 27, 2006; Revised Manuscript Received February 15, 2007 ; E-mail: mmaroney@chemistry.umass.edu

Abstract: Studies of the transcriptional repression of the Ni-specific permease encoded by the P_{nik} operon by *Escherichia coli* NikR using a LacZ reporter assay establish that the NikR response is specific to nickel *in vivo*. Toward understanding this metal ion-specific response, X-ray absorption spectroscopy (XAS) analysis of various M-NikR complexes (M = Co(II), Ni(II), Cu(II), Cu(I), and Zn(II)) was used to show that each high-affinity binding site metal adopts a unique structure, with Ni(II) and Cu(II) being the only two metal ions to feature planar four-coordinate complexes. The results are consistent with an allosteric mechanism whereby the geometry and ligand selection of the metal present in the high-affinity site induce a unique conformation in NikR that subsequently influences DNA binding. The influence of the high-affinity metal on protein structure was examined using hydrogen/deuterium (H/D) exchange detected by liquid chromatography-electrospray ionization mass spectrometry (LC-ESI-MS). Each NikR complex gives rise to differing amounts of H/D exchange; Zn(II)- and Co(II)-NikR are most like apo-NikR, while the exchange time course is substantially different for Ni(II) and to a lesser extent for Cu(II). In addition to the high-affinity metal binding site, *E. coli* NikR has a low-affinity metal-binding site that affects DNA binding affinity. We have characterized this low-affinity site using XAS in heterobimetallic complexes of NikR. When Cu(II) occupies the high-affinity site and Ni(II) occupies the low-affinity site, the Ni *K*-edge XAS spectra show that the Ni site is composed of six N/O-donors. A similar low-affinity site structure is found for the NikR complex when Co(II) occupies the low-affinity site and Ni(II) occupies the high-affinity site, except that one of the Co(II) ligands is a chloride derived from the buffer.

Introduction

Escherichia coli NikR is a homotetrameric, nickel-responsive regulatory protein that is a member of the ribbon-helix-helix family of transcriptional regulators.[1,2] NikR and the recently discovered RcnR protein[3] are involved in controlling the concentration of the intracellular nickel pool in *E. coli*, which is primarily targeted to the anaerobically expressed hydrogenase isozymes.[4] Nickel ions are imported via the ATP-dependent NikABCDE nickel transporter.[5] Modest amounts of nickel are required to satisfy hydrogenase activity requirements, while higher concentrations are toxic.[6] When the hydrogenase nickel requirements are satisfied, available nickel ions load into NikR, resulting in its increased affinity for the $P_{nikABCDE}$ promoter region, repressing the transcription of the NikABCDE nickel permease, thereby halting nickel import via this route.[4,5,7]

NikR appears to provide a common, though not universal, mechanism for coupling transcriptional regulation to intracellular nickel status. NikR homologs have been found in many bacteria and archaea,[8] though as demonstrated in *Helicobacter pylori*, the regulatory functions of NikR may vary. In *H. pylori*, NikR represses transcription of the nickel importer NixA, but it exhibits an additional regulatory function by inducing P_{ureA} transcription with increasing nickel concentrations.[9,10] Additionally, NikR demonstrates regulatory control over the outer membrane proteins FepA3 (HP 1400) and FrpB4 (HP1 1512), which are repressed by NikR at high intracellular Ni concentrations.[11,12]

The presence of two distinct metal binding sites in *E. coli* NikR is inferred from several studies.[13,14] The "high-affinity"

[†] University of Massachusetts.
[‡] Washington University.

(1) Chivers, P. T.; Sauer, R. T. *Protein Sci.* **1999**, *8*, 2494−500.
(2) Chivers, P. T.; Sauer, R. T. *J. Biol. Chem.* **2000**, *275*, 19735−41.
(3) Iwig, J. S.; Rowe, J. L.; Chivers, P. T. *Mol. Microbiol.* **2006**, *62*, 252−62.
(4) Rowe, J. L.; Starnes, G. L.; Chivers, P. T. *J. Bacteriol.* **2005**, *187*, 6317−23.
(5) Navarro, C.; Wu, L. F.; Mandrand-Berthelot, M. A. *Mol. Microbiol.* **1993**, *9*, 1181−91.
(6) Wu, L. F.; Navarro, C.; de Pina, K.; Quenard, M.; Mandrand-Berthelot, M. A. *Environ. Health Perspect.* **1994**, *102* (Suppl 3), 297−300.
(7) Wu, L. F.; Mandrand-Berthelot, M. A.; Waugh, R.; Edmonds, C. J.; Holt, S. E.; Boxer, D. H. *Mol. Microbiol.* **1989**, *3*, 1709−1718.
(8) Rodionov, D. A.; Hebbeln, P.; Gelfand, M. S.; Eitinger, T. *J. Bacteriol.* **2006**, *188*, 317−27.
(9) Contreras, M.; Thiberge, J. M.; Mandrand-Berthelot, M. A.; Labigne, A. *Mol. Microbiol.* **2003**, *49* (4), 947−63.
(10) van Vliet, A. H.; Ernst, F. D.; Kusters, J. G. *Trends Microbiol.* **2004**, *12*, 489−94.
(11) Ernst, F. D.; Stoof, J.; Horrevoets, W. M.; Kuipers, E. J.; Kusters, J. G.; van Vliet, A. H. *Infect. Immun.* **2006**, *74*, 6821−6828.
(12) Davis, G. S.; Flannery, E. L.; Mobley, H. L. *Infect. Immun.* **2006**, *74*, 6811−6820.
(13) Chivers, P. T.; Sauer, R. T. *Chem. Biol.* **2002**, *9*, 1141−8.

site is located near the C-terminal, tetrameric interface of each subunit, and is associated with seven invariant residues (Y60, H62, H76, H87, H89, C95, and E97). It has a $K_d = 6.8$ pM for Ni(II) and a stoichiometry of four per tetramer.[13] Data from X-ray absorption spectroscopy (XAS) and crystal structure analysis of the C-terminal domain of *E. coli* NikR reveal a four-coordinate square-planar Ni(II) site with a ligand environment consisting of three imidazole N-donors from invariant histidine residues (H76′ from a neighboring side chain, H87, and H89) and an additional S-donor from the invariant cysteine residue (C95).[15,16] The three remaining invariant residues (Y60, H62, and E97) are located within 6.8 Å of this nickel site. Virtually identical sites have been established in *Pyrococcus horikoshii* NikR from crystallographic data of the full-length protein[17] and in *H. pylori* using XAS analysis and crystallography.[18,19] The "low-affinity" site in *E. coli* NikR has reported K_d's ranging from μM to nM[13,14] and has an apparent stoichiometry of two per tetramer on the basis of inferences from crystal structures[17,20] and the analytical data presented below. The recent publication of several structures of the *P. horikoshii* NikR protein shows several potential metal binding sites and suggests that the low-affinity sites lie near the interface of the C-terminal domain and the DNA binding domain.[17] In *E. coli* NikR, tighter DNA binding accompanied by a larger protein-DNA footprint have been reported *in vitro* when nickel is present at a sufficiently high concentration to occupy all sites.[13] However, these low-affinity sites do not appear to be present in *H. pylori* NikR,[18,19,21] and their specific *in vivo* function and metal specificity remain to be elucidated.

NikR binds many first-row transition-metal ions *in vitro* and the binding affinities follow the Irving−Williams series (Co(II) < Ni(II) < Cu(II) > Zn(II), with Cu(II) binding 1000× tighter than Ni(II)).[22] Thus, the origin of any nickel-specific response does not lie in the thermodynamics of complex formation. Pennella *et al.*[23] have suggested that some metalloregulators may operate by allowing the metal geometry or choice of ligands to influence the protein structure. The possibility that metal site occupancy influences the NikR protein structure is suggested by the number of crystal structures of *P. horikoshii* NikR[17] and *E. coli* NikR[16,20] in various DNA bound and free states.

Herein, we establish the nickel-specific response of *E. coli* NikR protein *in vivo* using a LacZ reporter assay and examine the metal site structures of NikR proteins with different metals in the high-affinity site for insights into the mechanism that gives rise to the Ni-specific biological response. The structures of complexes formed using the high-affinity metal-binding sites were investigated using XAS to examine the role of coordination geometry and ligand selection in a series of metal-substituted NikR proteins, M−NikR (M = Co(II), Ni(II), Cu(II), Cu(I), and Zn(II)). The response of protein conformation to metal binding was addressed using hydrogen−deuterium exchange, as measured by LC-ESI-MS.

By taking advantage of the difference in K_d's of the two sites and the relative affinities of metals for the higher affinity binding site compared to the lower affinity binding site, we have been able to study NikR proteins with Ni(II) in the high-affinity site and Co(II) in the low-affinity site (NiCo-NikR) and Cu(II) in the high-affinity site and Ni(II) in the low-affinity site (CuNi-NikR). This allowed us to use XAS to examine the structure of the low-affinity metal-binding site of *E. coli* NikR and to investigate the structural effects on the high-affinity binding site because of occupancy of the low-affinity site.

Experimental Section

LacZ Reporter Assays. β-Galactosidase assays were performed on anaerobically grown cultures in microfuge tubes as previously described.[4] *E. coli* K12 strain RZ4500 (PC113) was used as wild-type and isogenic mutants Δ*nikR* (PC269), Δ*nikA* (PC237), and Δ*nikR*, Δ*corA* (PC477) have been described previously.[4] Cells were grown in a defined M63 minimal medium containing 1 mM $MgCl_2$, 5 μM $FeCl_2$, 1 μM $ZnCl_2$, and 100 nM each of $MnCl_2$, Na_2MoO_4, and Na_2SeO_3 added before sterile filtration. Glucose (0.25% w/v) was added as a carbon source and, when indicated, 10 mM sodium formate or potassium nitrate was added to modulate P_{nik} expression levels.[4] Data were fit as described previously.[4]

Metal-toxicity limits in M63 minimal defined medium were determined individually for the biologically relevant first-row transition metals added as chloride salts: $MnCl_2$ (10 μM), $FeCl_2$ (20 μM), $CoCl_2$ (1 μM), $NiCl_2$ (1 μM), $CuCl_2$ (10 μM), and $ZnCl_2$ (100 μM). The concentration in parenthesis was the highest at which less than a 10% reduction in OD_{600} was observed after overnight (14 h) anaerobic growth at 37 °C.

Nickel Accumulation Assay. Nickel accumulation was measured after overnight growth as described previously using $^{63}NiCl_2$.[3] Cells were grown overnight with 5 nM $^{63}NiCl_2$ in the presence or absence of 1 μM $CoCl_2$. Cells were harvested and washed, and ^{63}Ni content was determined by liquid scintillation counting.

Metal-Substituted NikR Proteins. *E. coli* apo-NikR was prepared by incubation with 50 mM EDTA (0.5 M stock [pH 8.0]) at 4 °C for 2−4 days using protein that was overexpressed in *E. coli* DL-41(DE3)pLysS or DL-41(DE3) and was isolated as previously described.[2,13] For hydrogen/deuterium (H/D) exchange studies, apo-NikR samples (100 μM in 20 mM Tris (pH 8.0), 100 mM NaCl) were diluted by stepwise addition of 100 μM M(II) chloride stocks to a final concentration of 50 μM NikR and 50 μM M(II). Samples were equilibrated overnight at room temperature (23 °C). A small amount of protein precipitation was observed, likely because of metal binding at the protein surface,[24] and was removed by centrifugation at 12 000*g* for 4 min. Unbound metal was removed by desalting using a P6 spin column (Bio-Rad) equilibrated with the buffer described above. Metal-binding stoichiometry was confirmed using the published extinction coefficients for the Ni(II)−NikR, Cu(II)−NikR, and Co(II)−NikR complexes[22] or by the PAR assay for Zn(II)−NikR.[25] Metal-substituted NikR proteins used for XAS studies were prepared by first buffer exchanging apo-NikR into a low-salt buffer (20 mM Tris, 100 mM NaCl, pH 8.3) that had been treated with Chelex-100 to remove metal ions. Aqueous 50 mM stock solutions were prepared from the $[Co(H_2O)_6]Cl_2$, $[Cu(H_2O)_6]Cl_2$, and $[Zn(H_2O)_6]Cl_2$ salts (Fisher Scientific) and were added directly to ∼250 μM protein solutions in the

(14) Bloom, S. L.; Zamble, D. B. *Biochemistry* **2004**, *43*, 10029−38.
(15) Carrington, P. E.; Chivers, P. T.; Al-Mjeni, F.; Sauer, R. T.; Maroney, M. *Nat. Struct. Biol.* **2003**, *10*, 126−30.
(16) Schreiter, E. R.; Sintchak, M. D.; Guo, Y.; Chivers, P. T.; Sauer, R. T.; Drennan, C. L. *Nat. Struct. Biol.* **2003**, *10*, 794−9.
(17) Chivers, P. T.; Tahirov, T. H. *J. Mol. Biol.* **2005**, *348*, 597−607.
(18) Benanti, E. L.; Iwig, J. S.; Leitch, S.; Meheen, A.; Maroney, M. J.; Chivers, P. T. unpublished results.
(19) Dian, C.; Schauer, K.; Kapp, U.; McSweeney, S. M.; Labigne, A.; Terradot, L. *J. Mol. Biol.* **2006**, *361*, 715−30.
(20) Schreiter, E. R.; Wang, S. C.; Zamble, D. B.; Drennan, C. L. *Proc. Natl. Acad. Sci. U.S.A.* **2006**, *103*, 13676−81.
(21) Abraham, L. O.; Li, Y.; Zamble, D. B. *J. Inorg. Biochem.* **2006**, *100*, 1005−14.
(22) Wang, S. C.; Dias, A. V.; Bloom, S. L.; Zamble, D. B. *Biochemistry* **2004**, *43*, 10018−10028.
(23) Pennella, M. A.; Shokes, J. E.; Cosper, N. J.; Scott, R. A.; Giedroc, D. P. *Proc. Natl Acad. Sci. U.S.A.* **2003**, *100*, 3713−3718.
(24) Fauquant, C.; Diederix, R. E.; Rodrigue, A.; Dian, C.; Kapp, U.; Terradot, L.; Mandrand-Berthelot, M. A.; Michaud-Soret, I. *Biochimie* **2006**, *88*, 1693−705.
(25) Hunt, J.; Neece, S.; Ginsburg, A. *Anal. Biochem.* **1985**, *146*, 150−157.

following M:protein ratios: Cu(II), 1:1; Zn(II), 0.9:1; Co(II), 0.8:1. The Co(II)−NikR sample had a trace amount of Ni (∼1%) that is visible in the Co(II)−NikR XAS spectrum. This could be a result of either incomplete removal of nickel during incubation with EDTA or trace contamination of the $[Co(H_2O)_6]Cl_2$ salt with a small amount of nickel. Addition of substoichiometric amounts of Co(II) and Zn(II) significantly reduced precipitation of the protein. The final complexes were incubated with Chelex-100 to remove any nonspecifically bound metal. Aliquots were then taken for metal analysis by inductively coupled plasma atomic emission spectroscopy (ICP-AES). Protein concentrations were determined under denaturing conditions using the molar absorptivity $\epsilon_{276} = 4490\ M^{-1}\ cm^{-1}$. The combined results of the metal and protein analysis gave M:protein ratios of 0.9:1, 0.9:1; and 1.2:1, respectively, for the Co(II), Cu(II), and Zn(II) substituted NikR samples used for XAS studies. Cu(I)−NikR was prepared in a Coy (Coy Laboratory Products Inc., Grass Lakes, MI) anaerobic chamber by incubating Cu(II)−NikR with 10 mM DTT for ∼1 h and then buffer exchanging into low-salt buffer using a microspin concentrator (Vivascience). The Cu(I)−NikR was analyzed by ICP-AES post-reduction and the final M:protein ratio was 0.3:1. Samples of metal-substituted proteins were concentrated to a metal concentration of ∼1−5 mM for XAS analysis. Final concentration and freezing of the Cu(I)−NikR aliquot for XAS analysis was done under an anaerobic atmosphere.

Bimetallic NikR Proteins. Samples of Cu(II)−NikR or Ni(II)−NikR were prepared as described above, were concentrated (to ∼2 mM), and then were incubated with 1.1 equiv of the P_{nik} operon per tetramer overnight at room temperature. The resulting M−NikR−DNA complexes (M = Cu(II) or Ni(II)) were then diluted 10 000-fold with low-salt buffer. The concentrations used were such that 99% of the protein was complexed to DNA under the most dilute conditions given the binding affinities reported.[14] Mass spectral studies confirm that a weak NikR−DNA complex is obtained in the absence of Ni(II) ions and that strong complexation is observed in the presence of four high-affinity site Ni(II) ions using the same DNA construct.[26] Analysis of the retention times of the components and the NikR−DNA complex using the same DNA construct show that the complex survives gel filtration (see Supporting Information). Aqueous solutions of 10 mM $NiCl_2$ and $CoCl_2$ were prepared. In multiple aliquots, 0.45 mol equiv of $NiCl_2$ was added to the Cu(II)−NikR and 0.45 mol equiv $CoCl_2$ was added to the Ni(II)−NikR. The total amount of metal added to the M−NikR−DNA complexes was calculated on the basis of two low-affinity binding sites per tetramer. The resulting disubstituted NikR−DNA complexes were immediately desalted on a 4 mL capacity Zebra spin desalt column (Pierce Biotechnology) that was pre-equilibrated with low-salt buffer. The sample prepared with bromide in place of chloride was prepared as above, except $MgBr_2$ was substituted for $MgCl_2$ when annealing the P_{nik}, and NaBr and HBr were used in place of NaCl and HCl, respectively, in the low-salt buffer. The chloride contributed from the metal salts was considered negligible, as the final concentration was less than 0.5%. Each dimetalated NikR was analyzed for metal content using ICP-AES, and protein concentration was determined prior to DNA addition under denaturing conditions with a molar absorptivity $\epsilon_{276} = 4490\ M^{-1}cm^{-1}$. For each NiCo−NikR (±$Br^-$), the molar ratio of Ni:Co was 1.9:1. For CuNi−NikR, the molar ratio of Cu:Ni was 1.6:1. Attempts to prepare samples with metals loaded in the low-affinity sites in the absence of DNA gave irreproducible metal analyses that are low for the low-affinity site metal and formed significantly more precipitate upon addition to the low-affinity metal, suggesting that the site is not well formed in the absence of DNA. Example analyses obtained in the absence of DNA were Cu:Ni = 4:1 and 18:1, and Ni:Co = 83:1.

Electron Paramagnetic Resonance (EPR) Data Collection. EPR spectra of Cu(II)−NikR and CuNi−NikR were obtained using a Bruker ESP 300 X-band spectrometer. Samples in polycarbonate XAS cuvettes were inserted into a finger dewar filled with liquid N_2 for data collection. Both spectra were collected prior to XAS analysis.

XAS Data Collection. XAS data was collected under dedicated conditions at either Stanford Synchrotron Radiation Laboratory (SSRL, beam line 9-3) or at the National Synchrotron Light Source (NSLS, beam line X9b) at Brookhaven National Laboratory. The data from Cu(I)−NikR and the bimetallic NiCo−NikR with Br^- in place of Cl^- were collected at SSRL. Each sample was syringed into a polycarbonate sample holder with a kapton tape window and was rapidly frozen in liquid N_2. The samples were analyzed at 10 K using a liquid He cryostat. The ring conditions were 3 GeV and 80−100 mA. Beam line optics consisted of a Si(220) double-crystal monochromator and two rhodium-coated mirrors, a flat mirror before the monochromator for harmonic rejection and vertical collimation, and a second toroidal mirror after the monochromator for focusing. X-ray fluorescence was collected using a 30-element Ge detector (Canberra). Scattering was minimized by placing a set of Soller slits with a Z-1 element filter between the sample chamber and the detector.

The remaining data were collected on beam line X9b at NSLS. Each sample was pipetted into a polycarbonate sample holder and then was rapidly frozen in liquid N_2. Samples were then inserted into an aluminum frame with a kapton tape window that was held at ∼50 K by a He displex cryostat. Data were collected under ring conditions of 2.8 GeV and 120−300 mA using a sagitally focusing Si(111) double-crystal monochromator. Harmonic rejection was accomplished with a Ni-coated focusing mirror. X-ray fluorescence was collected using a 13-element Ge detector (Canberra).

For all samples, X-ray absorption near-edge spectroscopy (XANES) was collected from ±200 eV relative to each edge. Extended X-ray absorption fine structure (EXAFS) was collected to 13.5−16 k above the edge energy (E_0). The X-ray energy for each K_α-edge was calibrated to the first inflection point of the corresponding metal foil: Co, 7709.5 eV; Ni, 8331.6 eV; Cu, 8980.3 eV; and Zn, 9660.7 eV. Sample integrity during exposure to X-ray radiation was determined by monitoring changes in the edge energy and XANES spectrum over sequential scans. No significant photoreduction or oxidation was observed except for changes in the Cu(II) XANES spectrum from CuNi−NikR that indicate photoreduction in the beam. The changes were particularly pronounced if Ni *K*-edge data was collected prior to collection of the Cu *K*-edge. (see Results and Supporting Information for CuNi−NikR samples).

Data Reduction and Analysis. XAS data reduction and analysis was performed using EXAFS123,[27] with the graphics produced using Igor Pro (WaveMetrics Version 5.0). XANES analysis was done by fitting a cubic function to the baseline in the pre-edge region of the spectra and using a 70% Gaussian and 25% Lorenzian function to fit the rise in fluorescence occurring at the edge. Gaussian functions were added for transitions occurring at lower energy and the areas of the Gaussians were taken to be the peak areas. An average of four scans was used for XANES analysis.

For EXAFS analysis, four to eight scans were averaged to generate the EXAFS spectrum for each sample. For each data set, the averaged spectrum was background-corrected and normalized using a three-section cubic spline to fit the background in the pre-edge and post-edge regions. The data were converted to *k*-space using the relationship $[2m_e(E - E_0)/\hbar^2]^{1/2}$ (where m_e is the mass of the electron, $\hbar$ is Plank's constant divided by 2π, and E_0 is the threshold energy of the absorption edge, which was chosen to be 7723 eV for Co, 8340 eV for Ni, 8990 eV for Cu, and 9670 eV for Zn. Least-squares fitting of the EXAFS data over a *k*-range of 2−12 $Å^{-1}$ for Co; 2−12.5 $Å^{-1}$ for Ni, Cu(II), and Zn; and 2−14 $Å^{-1}$ for Cu(I) was first done using Fourier-filtered data to get a first approximation of the fits and then was further refined using unfiltered data for the final fits presented in Figures 2 and 4 and Tables 1 and 2. The upper limits of the *k*-space range of the data sets

(26) Kaltashov, I. A.; Zhang, M.; Eyles, S. J.; Abzalimov, R. R. *Anal. Bioanal. Chem.* **2006**, *386*, 472−81.

(27) Padden, K. M.; Krebs, J. F.; MacBeth, C. E.; Scarrow, R. C.; Borovik, A. S. *J. Am. Chem. Soc.* **2001**, *123*, 1072−1079.

were limited by either the presence of the metal with the subsequent K-edge energy or by noise. Integer values of the number of scattering atoms in each shell were used without refinement. This led to three free-running parameters for fits of the first coordination sphere: r (bond distance), σ^2 (disorder parameter), and E_0 (phase shift). Fits with more than one shell of N/O scattering atoms in the first coordination sphere were refined by using only one value of σ^2 and E_0 for the different shells of N/O-donors, and all possible combinations of N/O and S donors were examined for two to seven ligands in the first coordination sphere. The program FEFF, version 8.0,[28] was used to calculate both the single-scattering parameters for Me−N, Me−S, and second-coordination sphere Co−C_{imd} and the multiple-scattering parameters for histidine imidazole ligands using structural information from previously published crystal structures.[29−34] Imidazole ligands were fit as rigid rings by adjusting only the M−N distance, σ^2, and E_0 while retaining the ring geometry as previously described.[35] The values for σ^2 and E_0 were constrained to be the same as the M−N/O scatterers. Histidine ligands were "counted" by adding integer values of imidazole ligands to trial fits, and evaluated using the effect on the goodness of fit (GOF) and σ^2 values. The number of imidazole ligands found in this manner has an estimated error of 25% on the basis of studies of model complexes, which is the same error obtained for estimates of the number of scattering atoms in the first-coordination sphere from EXAFS analysis because of correlations between N and σ^2 for a given shell. For Co(II), this approach failed to give acceptable fits, so the procedure was modified to use single-scattering parameters for imidazole C atoms in the second-coordination sphere and multiple-scattering parameters for the C and N atoms in the third-coordination sphere. This had the effect of not holding the imidazole rings as a rigid unit by allowing the r for the second-coordination sphere C-atoms to refine independently from either the M−N distance or the third-coordination sphere. This additional degree of freedom was sufficient to give acceptable fits for the Co(II) samples.

Hydrogen/Deuterium Exchange Reaction. H/D exchange and mass spectrometry methods were adapted from the literature.[36,37] H/D exchange reactions were carried out by incubating 10 μM NikR samples (apo- or with Ni(II), Cu(II), Co(II), or Zn(II) bound) at room temperature (23 °C). At 0 min, the sample was diluted 10-fold by addition of room-temperature D_2O, yielding 1 μM protein in 90% D_2O. Nineteen-microliter aliquots were removed and placed in a prechilled 0.5-mL microfuge tube containing 1 μL of 0.1 M HCl. The sample was immediately mixed and dipped into a dry ice/ethanol bath for 15 s to freeze the sample and to quench the H/D exchange reaction. Frozen samples were immediately transferred to −80 °C and were stored for 1−5 days.

LC-ESI Mass Spectrometry. Samples were thawed in a water bath (22 °C) with swirling for 30 s and then were immediately loaded into a six-port valve in an ice-bath containing an Opti-Guard C18 desalting column (10 mm × 1 mm i.d., P. J. Corbert Associates, Inc., St. Louis) equilibrated with prechilled 0.1% tri-fluoroacetic acid (TFA) in water (pH 2.5). The column-bound protein was washed with 200 μL of ice-cold 0.1% TFA in water. The protein was eluted using 30 μL/min isocratic flow of prechilled 80:19.7:0.3 (v/v/v) methanol/water/TFA (pH ~2.5), and the flow was directed into a Micromass Q-TOF Ultima GLOBAL mass spectrometer operated in the positive ion mode. The instrument settings were as follows: capillary voltage, 3.4 kV; TOF voltage, 10.1 kV; source temperature, 80 °C; desolvation temperature, 200 °C; cone gas flow, 40 L/h; and desolvation gas flow, 400 L/h. The TOF operated at 10 000 mass resolving power between m/z 600 and m/z 1400, the range in which NikR monomer peaks are detected. Normally, between 10 and 20 scans were summed for molecular mass analysis with MassLynx 4.0 using the maximum entropy algorithm (MaxEnt1 in MassLynx 4.0). The entire protein signal used for analysis was eluted and collected within 2 min of loading on the desalting column.

Synthetic P_{nik} Operator. Oligonucleotides were purchased from Integrated DNA Technologies (Coralville, IA) and were used without further purification. Four oligos were used to construct the 50-bp P_{nik} operon. Each oligo was resuspended in 100 μL of DNA buffer (10 mM Tris, 1 mM $MgCl_2$, pH 8.0) and was heated to 80 °C for 10 min. Equimolar amounts of each pair (5′-ACAGGTAATCAGTATGAC-GAA-3′ with 5′-TTTAAGTATTCGTCATACTGATTACCTGT-3′) and (5′-TACTTAAAATCGTCATACTTATTTCCGCC-3′ with 5′-GGCG-GAAATAAGTATGACGAT-3′) were combined and allowed to cool to room temperature (60−90 min) and then dried. Each half was then resuspended in 100 μL ddH_2O, and the halves were mixed in equimolar amounts. The combined DNA was heated to 37 °C for 10 min and then was cooled to room temperature (30 min) and was placed on ice for ~30 min. The annealed DNA fragment was dried and then resuspended in ~60 μL ddH_2O to make DNA solutions with a concentration of (10−15 mM) appropriate for XAS experiments.

Results

Metal-Dependent Effects on NikR-Regulation of $P_{nikABCDE}$ Expression. *In vivo* metal-dependent P_{nik} expression was examined using a LacZ reporter assay, and cells were grown in defined minimal medium conditions to which different first-row transition M(II) chloride salts were added. With the exception of Ni(II), none of the metals resulted in repression of P_{nik} expression (Figure 1A). Interestingly, 1 μM Co(II) resulted in 50% higher P_{nik} expression levels, which could result from an inhibition of NikR function. The effect of high (near toxic) divalent metal concentration on the Ni-dependent repression of $P_{nikABCDE}$ was also measured. These concentrations were determined empirically for the growth medium used in this study (see Experimental Section). No effects on nickel-dependent NikR function were observed except in the presence of 1 μM Co(II). Here, half-maximal repression of nikABCDE was shifted to a slightly higher nickel concentration, and the repression curve showed an apparent increase in cooperativity (K_{Ni} = 36 nM, n = 1.72 vs K_{Ni} = 8.6 nM, n = 1 for nickel alone or with the other metals) (Figure 1B). To determine whether metals could have synergistic or cumulative effects on P_{nik} expression, LacZ activity was assayed in the presence of all metals listed, each at their near toxic concentration. The Co(II) effect was observed, and nickel-dependent repression under these conditions resembled that for Co(II) alone (data not shown). Thus, not only is NikR function not blocked by these metals, but they also must not interfere with Ni import or the Co(II) effect.

Previous experiments have shown that NikR function is sensitive to perturbations in nickel homeostasis. Increased NikR function at low nickel concentrations (<10 nM) is directly correlated with decreases in hydrogenase expression[4] as well as decreased nickel efflux.[3] To determine whether the Co(II) effect was linked to NikR, P_{nik} expression was examined in M63

(28) Ankudinov, A. L.; Ravel, B.; Rehr, J. J.; Conradson, S. D. *Phys. Rev. B* **1998**, *58*, 7565−7576.
(29) Van Ingen Schenau, A. D. *Acta Crystallogr., Sect. B* **1975**, *31* (Nov 15), 2736−2738.
(30) Rosenfield, S. G.; Armstrong, W. H.; Mascharak, P. K. *Inorg. Chem.* **1986**, *25*, 3014−3018.
(31) Mcfadden, D. L.; Mcphail, A. T.; Garner, C. D.; Mabbs, F. E. *J. Chem. Soc., Dalton Trans.* **1975**, 263−268.
(32) Corwin, D. T.; Koch, S. A. *Inorg. Chem.* **1988**, *27*, 493−496.
(33) Clegg, W.; Acott, S. R.; Garner, C. D. *Acta Crystallogr., Sect. C: Cryst. Struct. Commun.* **1984**, *40*, 768−769.
(34) Bombieri, G.; Forsellini, E.; Delpra, A.; Tobe, M. L.; Chatterjee, C.; Cooksey, C. J. *Inorg. Chim. Acta* **1983**, *75*, 93−101.
(35) Davidson, G.; Choudhury, S. B.; Gu, Z.; Bose, K.; Roseboom, W.; Albracht, S. P.; Maroney, M. J. *Biochemistry* **2000**, *39*, 7468−79.
(36) Zhu, M. M.; Rempel, D. L.; Gross, M. L. *J. Am. Soc. Mass Spectrom.* **2004**, *15*, 388−97.
(37) Zhu, M. M.; Rempel, D. L.; Zhao, J.; Giblin, D. E.; Gross, M. L. *Biochemistry* **2003**, *42*, 15388−97.

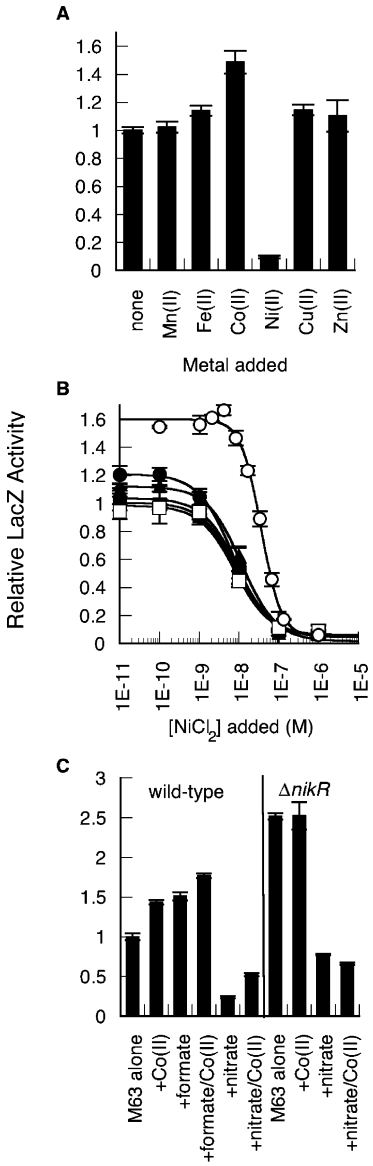

Figure 1. Effects of metals on NikR-dependent regulation of $P_{nikABCDE}$ expression. P_{nik}-lacZ expression is reported relative to wild-type without any metal added (3500−4000 Miller units). (A) P_{nik}-lacZ expression with different metals added at near toxic concentrations (see Experimental Section). (B) Metal-dependent effects on nickel-dependent repression of P_{nik}-lacZ expression. Ni(II) alone, filled squares; Cu(II), filled circles; Fe(II), filled triangles; Mn(II), filled diamonds; Zn(II), open squares; Co(II), open circles. All other metals had no effect within the limits of detection of this assay. (C) The Co(II) effect under different anaerobic growth conditions. Cells were grown without any added Ni(II).

growth medium containing 10 mM nitrate, where the baseline P_{nik} expression is reduced because of the actions of NikR and the nitrate-responsive two-component system NarLX,[4] allowing any Co(II) dependent change in induction to be more easily detected. The Co(II) effect was only observed when NikR was present (Figure 1C), indicating that Co(II) acts by inhibiting NikR function in some way. To test whether Co(II) was perturbing intracellular nickel levels, ^{63}Ni accumulation was measured in the presence and absence of 1 μM $CoCl_2$. Co(II) resulted in a significant decrease in intracellular nickel levels after overnight growth (487 ± 29 Ni/cell, four replicates vs 358 ± 27 Ni/cell, five replicates). These results suggested that the decrease in NikR function was due to an indirect effect of Co(II) on NikR because of decreased Ni import. Deletion of the *rcnR* and *rcnA* genes involved in nickel and cobalt efflux did not alter the Co(II) effect on P_{nik}-lacZ expression, confirming that intracellular Co levels did not impact NikR function. These results suggest that NikR function in *E. coli* is highly nickel-specific even in the presence of other transition metals at levels that induce stress responses in their respective metal homeostasis pathways (e.g., for Cu and Zn).[38,39]

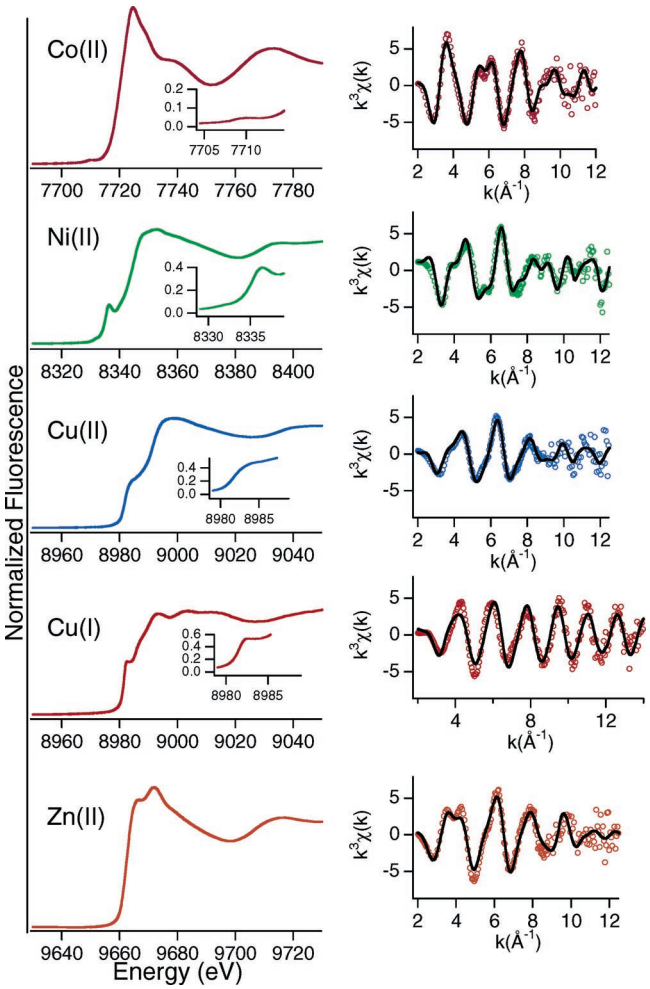

Figure 2. High-affinity site metal-substituted NikR *K*-edge XAS. Left: XANES spectra. Right: Unfiltered EXAFS data in circles and fits from Table 1. The range of the *k*-space fits is 2−12 Å^{-1} for Co(II); 2−12.5 Å^{-1} for Ni(II), Cu(II), and Zn(II); and 2−14 Å^{-1} for Cu(I).

The High-Affinity Site. XANES. The results of *K*-edge XAS studies of the high-affinity site metal-substituted NikR proteins are summarized Figure 2 and Table 1. XANES analysis can provide information regarding the coordination number and geometry of each metal site. All metal ions with a vacancy in the 3d manifold exhibit peaks in the XANES region that can be assigned as involving 1s → 3d electronic transitions. Ni(II)−NikR shows two distinct pre-edge features; the peak at ~8330 eV is assigned to a 1s → 3d transition (peak area = 0.0076(6) eV), and the additional resolved pre-edge transition near 8338 eV is assigned to a process involving a 1s → 4p_z electronic transition.[40] The small area of the 1s → 3d transition indicates a centrosymmetric arrangement of ligands, and a resolved 1s

(38) Outten, F.; Huffman, D.; Hale, J.; O'Halloran, T. *J. Biol. Chem.* **2001**, *276*, 30670−7.
(39) Yamamoto, K.; Ishihama, A. *J. Bacteriol.* **2005**, *187*, 6333−40.
(40) Eidness, M. K.; Sullivan, R. J.; Cramer, S. P.; Scott, R. A. *The Bioinorganic Chemistry of Nickel*; VCH: Deerfield Beach, FL, 1988; Chapter 4.

Table 1. XAS Analysis for High-Affinity Site Metal-Substituted NikR Complexes

NikR complex	geometry	CN[a]	*N*[b]	*r* (Å)[c]	σ^2 ($\times 10^3$Å^{-2})[d]	ΔE_0 (eV)	GOF[e]
Co(II)	octahedral	6	3 Co−N_{imd}	2.047(4)	6.4(6)[f]	6.7(7)	0.95
			6 Co−C_{imd}	2.959(10)	5.8(8)	10.0(10)	
			3 Co−N/O	2.171(6)	[6.4]	[6.7]	
Ni(II)	planar	4	3 Ni−N_{imd}	1.905(3)	1.8(3)	11.8(5)	0.84
			1 Ni−S	2.130(6)	0.5(3)	−16.0(18)	
Cu(II)	planar	4	2 Cu−N_{imd}	1.928(8)	4.3(6)	5.0(10)	0.77
			1 Cu−N/O	2.100(28)	[4.3]	[5.0]	
			1 Cu−S	2.210(9)	4.3(9)	8.1(16)	
Cu(I)	trigonal	3	1 Cu−N_{imd}	2.130(16)	2.4(1)	12.5(11)	1.06
			1 Cu−N/O	2.036(14)	[2.4]	[12.5]	
			1 Cu−S	2.279(5)	1.7(2)	7.9(14)	
Zn(II)	tetrahedral	4	3 Zn−N_{imd}	1.990(6)	4.9(5)	2.9(7)	1.01
			1 Zn−S	2.229(8)	2.7(5)	1.3(22)	

[a] CN is the overall coordination number. [b] *N* is the number of bonds at a specific distance. [c] *r* (Å) is the bond distance. [d] σ^2 is the mean square disorder in the Ni−X distance, where X is the scattering atom. [e] GOF (goodness of fit) was calculated as described in the Experimental Section. The accuracy of distance determined by EXAFS for atoms in the first coordination sphere of the metal is limited to ±0.02 Å by the theoretical phase parameters; numbers in parentheses represent standard deviations from the least-squares fits. [f] Values of parameters in [] were constrained to be equal to those of other scattering atoms in the same shell.

→ $4p_z$ is diagnostic for a planar geometry.[41] Thus, the Ni(II) high-affinity site is four-coordinate and has a planar geometry, as previously reported.[15] Co(II)−NikR has a pre-edge peak assigned to a 1s → 3d transition at ∼7710 eV (peak area = 0.069(8) eV), where the small peak area also indicates a centrosymmetric environment and rules out tetrahedral and five-coordinate geometries.[27] Four-coordinate planar coordination is much less common for d^7 Co(II), and the absence of any other pre-edge feature is consistent with an octahedral ligand arrangement. For the CuNikR proteins, only d^9 Cu(II) can exhibit a 1s → 3d transition. However, there is only one vacancy in the 3d manifold for Cu(II), which gives rise to a very weak 1s → 3d peak intensity. Because of this, and because the peak overlaps with other pre-edge features, it is difficult to analyze. However, the other spectral features in the XANES spectrum can be used to determine the coordination environment.[42] The position of the edge allows for discrimination of the oxidation state. Tetragonal Cu(II) complexes show a low-energy absorption tail through the 8983−8985 eV region, as seen in Cu(II)−NikR. In contrast, Cu(I)−NikR has a resolved pre-edge transition at 8983 eV, and the position and the normalized intensity of this peak have been shown to vary with coordination number.[42] XANES arising from three-coordinate Cu(I) complexes has a pre-edge transition with a normalized intensity of ∼0.55 that falls between 8983 to 8984 eV. For four-coordinate complexes, the amplitude of this transition is greater than 0.6 in comparison to the normalized edge, and the maximum of the pre-edge feature falls between 8985 and 8986 eV.[42] The XANES observed for Cu(I)−NikR reveals a pre-edge transition with an intensity of 0.52 relative to the edge at 8982.6 eV, indicating a three-coordinate Cu(I) center. It is not possible to distinguish between trigonal planar and T-shaped geometries. Like Cu(I), Zn(II) is a d^{10} metal, and there are no holes in the 3d manifold to give rise to a 1s → 3d transition. XANES for Zn(II) is much less informative about coordination number and geometry than is the case for Cu(I), however a qualitative analysis of the XANES can provide information about the ligand donor atoms bound to Zn. Analysis of the "double-bump" feature of the white line with local maxima at ∼9664 eV and ∼9670 eV can be used to qualitatively determine the number of N-donors in comparison to S-donors.[43] If the Zn site is composed of strictly thiolate ligation, then the peak at ∼9664 eV is larger. The peak at ∼9670 eV increases as the ratio of N-donors to S-donors increases. In the Zn(II)-NikR, both peaks are present and the peak at ∼9670 eV is larger, indicating mixed N and S ligation that favors higher contribution from N ligands to the overall coordination sphere. Additionally, the intensity of the white line correlates with coordination number in Zn(II) XANES. For five- and six-coordinate complexes, the white line intensity reaches between 1.5 and 2. However, four-coordinate complexes all fall at approximately 1.2.[44] The white line in Zn(II)−NikR falls at an intensity of 1.2, consistent with a four-coordinate complex.

EXAFS. EXAFS analysis provides metal−ligand donor-atom distances within *ca.* 0.02 Å, indications of the types of donor atoms present (Z ± 1), and an estimate of the coordination number (±25%). EXAFS fitting results for M−NikR complexes are summarized in Table 1 and Figure 2. EXAFS results from the different M−NikR complexes show a variety of coordination environments arise that implicate all seven invariant residues associated with the high-affinity metal-binding site as potential ligands of the various metal ions. Ni(II)−NikR has been previously characterized by XAS and crystallography, which together establish that Ni(II) coordinates to the high-affinity site in a planar geometry composed of three N-donors from histidine residues (H76′, H87, and H89) and one S-donor from C95, where H76′ is contributed from another subunit.[15,16] The data analysis presented here is consistent with the prior XAS study[15] and is included here for comparison with other M−NikR proteins analyzed by the same procedure. The number of histidine ligands determined using multiple-scattering parameters and our histidine "counting" procedure (*vide supra*) for this Ni(II)−NikR data set is three (±25%). So, the Ni(II)−NikR is best fit with three N-imidazole donors at 1.90(2) Å and an additional S-donor at 2.13(2) Å. In contrast, the Co center of Co(II)−NikR is best fit as a six-coordinate complex composed strictly of N/O-donors (modeled here as N-donors). This is consistent with the XANES analysis (*vide supra*). Multiple-scattering analysis reveals that *ca.* three imidazole ligands are bound at an average bond distance of 2.05(2) Å, while the remaining three N/O donors are at an average bond distance of 2.14(2) Å.

The best fits of EXAFS data for Cu(II)−NikR are consistent with a four-coordinate metal site with the same ligand set found for Ni(II), however, only two of the N-donors could be modeled by imidazoles. This is consistent with the tetragonal geometry indicated by the XANES analysis and the EPR spectra (*vide infra*). Although the ligand selection and geometry is similar to Ni(II), the Cu(II) site is more distorted as a result of the lengthening one M−N/O by 0.05 Å and the M−S distance by 0.08 Å relative to the Ni(II) complex. The final best fits for

(41) Colpas, G. J.; Maroney, M. J.; Bagyinka, C.; Kumar, M.; Willis, W. S.; Suib, S. L.; Baidya, N.; Mascharak, P. K. *Inorg. Chem.* **1991**, *30*, 920−928.
(42) Kau, L. S.; Spirasolomon, D. J.; Pennerhahn, J. E.; Hodgson, K. O.; Solomon, E. I. *J. Am. Chem. Soc.* **1987**, *109*, 6433−6442.
(43) Clark-Baldwin, K.; Tierney, D. L.; Govindaswamy, N.; Gruff, E. S.; Kim, C.; Berg, J.; Koch, S. A.; Penner-Hahn, J. E. *J. Am. Chem. Soc.* **1998**, *120*, 8401−8409.
(44) Jacquamet, L.; Aberdam, D.; Adrait, A.; Hazemann, J. L.; Latour, J. M.; Michaud-Soret, I. *Biochemistry* **1998**, *37*, 2564−2571.

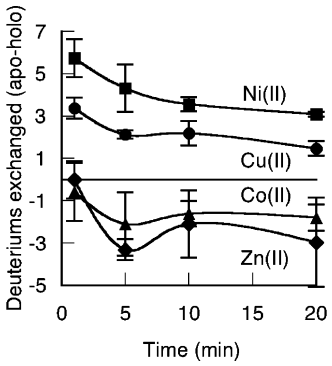

Figure 3. Hydrogen−deuterium exchange of metal-substituted NikRs measured by mass spectrometry. Data are plotted as the difference of apo- minus M(II)-substituted NikR determined by the average mass of the sample (see experimental section). Each point is the average of three separate samples. The different samples are labeled (Ni(II), squares; Cu(II), circles; Co(II), triangles; Zn(II), diamonds). Under these conditions, the apo-NikR sample has ∼80 deuteriums at $t = 1$ min and ∼94 at $t = 20$ min (133 residues per monomer).

Cu(II)−NikR are modeled by two N-imidazole ligands at 1.93(2) Å, one additional N/O donor at 2.10(3) Å, and a S-donor at 2.21(2) Å.

Upon reduction to Cu(I), both XANES and the EXAFS analysis are consistent with a three-coordinate Cu(I) center. The EXAFS analysis clearly shows that this results from the loss of one of the histidine ligands, presumably the one that is derived from another subunit (H76′). The final ligand selection for Cu(I) includes one Cu−N imidazole donor at 2.13(2) Å, an additional N/O-donor at 2.04(2) Å, and a S-donor at 2.28(2) Å. EXAFS of the Zn(II) center in Zn(II)−NikR is modeled by three N-imidazole donors at 1.99(2) Å and one S-donor at 2.23(2) Å. These bond lengths are consistent with Zn−N and Zn−S bond distances in a tetrahedral geometry.[32] In five- and six-coordinate complexes, these bond distances are longer (∼2.10−2.15 Å for Zn−N and ∼2.46−2.59 Å for Zn−S vectors).[44] The best EXAFS fit is for a five-coordinate complex, but because both XANES analysis and the bond lengths are consistent with a tetrahedral geometry, the four-coordinate fit is favored. Further, the difference between the four- and five-coordinate fits is small (GOF = 1.01 vs 0.96), and the σ^2 values increase for the five-coordinate model but are still in an acceptable range (see Supporting Information).

M(II)-Dependent Conformational Changes in NikR. Hydrogen/deuterium exchange (H/D exchange) provides a facile method to study protein conformation by monitoring the exchange of backbone amide protons. Measuring changes in backbone amide H/D exchange properties because of a ligand-induced conformational change is a well-established approach.[45−49] H/D exchange measured by mass spectrometry is used here to monitor the conformational response of the NikR protein to stoichiometric M(II) binding.

Figure 3 shows the changes in the H/D exchange time courses of NikR because of the conformational effects of metal binding. The data are plotted as the difference between apo deuterium content minus holo deuterium content. Each M(II)-substituted form of NikR has a different H/D exchange time course relative to apo-NikR suggesting that the conformational ensemble of each species is different. Ni(II)−NikR shows the largest difference relative to apo-NikR at each time point. The difference of ∼6 amu per monomer between apo-NikR and Ni(II)−NikR after 1 min of H/D exchange suggests that approximately six amide backbone positions per chain with relatively fast (<1 min) exchange rates in apo-NikR are more protected in the nickel-substituted protein. The time courses of H/D exchange observed for Co(II)−NikR and Zn(II)−NikR are similar to each other and more similar to apo-NikR. In contrast, Cu(II) reveals an H/D exchange time course that is distinct from, but similar to, Ni(II)−NikR, suggesting that the similar protein conformations adopted by Cu(II)− and Ni(II)−NikR are quite different than those adopted by the Co(II)−NikR and Zn(II)−NikR.

The Low-Affinity Site. XANES. Because Cu(II) binds 1000× tighter to the high-affinity site, when Ni(II) is added to Cu(II)−NikR, it can be preferentially loaded into the low-affinity site without displacing the Cu(II). Similarly, Co(II) can be loaded into the low-affinity site without displacing Ni(II) from the high-affinity site. Bimetallic NikR complexes in the presence of 50-bp P_{nik} operator DNA were made in this fashion and were characterized by XAS. The results of this study are shown in Figure 4 and Table 2. When Ni is bound to the low-affinity Cu(II)−NikR site, it binds in a completely different fashion in comparison with the structure of Ni(II) in the high-affinity site. There is a small 1s → 3d transition (peak area = 0.030(4) eV) indicating a centrosymmetric geometry, but the absence of a 1s → $4p_z$ transition is indicative of an octahedral ligand arrangement. A similar experiment was performed on a sample where Co(II) is preferentially loaded into the low-affinity site of Ni(II)−NikR. In the XANES analysis of this Co center, a 1s → 3d peak (area = 0.091(4)eV) is present. Without the presence of any additional feature, the XANES is also consistent with a six-coordinate Co(II) complex.[27]

EXAFS. The results of EXAFS analysis obtained on the bimetallic NikR complexes are listed in Table 2. The low-affinity Ni(II) site in CuNi−NikR is best fit with six N/O-donor ligands, consistent with XANES analysis. The observation of scattering from atoms at *ca.* 4 Å from the nickel center in Fourier-transformed EXAFS spectra (see Supporting Information) suggests the presence of imidazole donors from histadines (or possibly DNA bases). When imidazole ligands are added to the fits, the fits improve. The best fit is found for a ligand set comprised of two imidazole ligands with Ni−N distances of 1.99(2) Å and four additional N/O-donors at 2.11(2). The EXAFS data from the low-affinity Co(II) site in the NiCo−NikR is also consistent with a six-coordinate site, where the Co(II) center has a very similar ligand environment to the Ni(II) low-affinity site including *ca.* two histidine ligands, but differs by the presence of an apparent S(Cl)-donor in the Co(II) low-affinity site. The best fit found for the cobalt ion features a ligand set comprised of two imidazole ligands with Co−N distances of 1.93(2) Å, three additional N/O-donors at 2.14(3) Å, and an apparent S-donor at 2.22(2) Å.

The presence of a S(Cl)-donor ligand in the low-affinity Co complex is a little puzzling because there are only two cysteine

(45) Miranker, A.; Robinson, C.; Radford, S.; Aplin, R.; Dobson, C. *Science* **1993**, *262*, 896−900.
(46) Engen, J.; Gmeiner, W.; Smithgall, T.; Smith, D. *Biochemistry* **1999**, *38*, 8926−8935.
(47) Ceccarelli, C.; Liang, Z.-X.; Strickler, M.; Prehna, G.; Goldstein, B.; Klinman, J.; Bahnson, B. *Biochemistry* **2004**, *43*, 5266−5277.
(48) Busenlehner, L.; Codreanu, S.; Holm, P.; Bhakat, P.; Hebert, H.; Morgenstern, R.; Armstrong, R. *Biochemistry* **2004**, *43*, 11145−11152.
(49) Yang, J.; Garrod, S.; Deal, M.; Anand, G.; Woods, V.; Taylor, S. *J. Mol. Biol.* **2005**, *346*, 191−201.

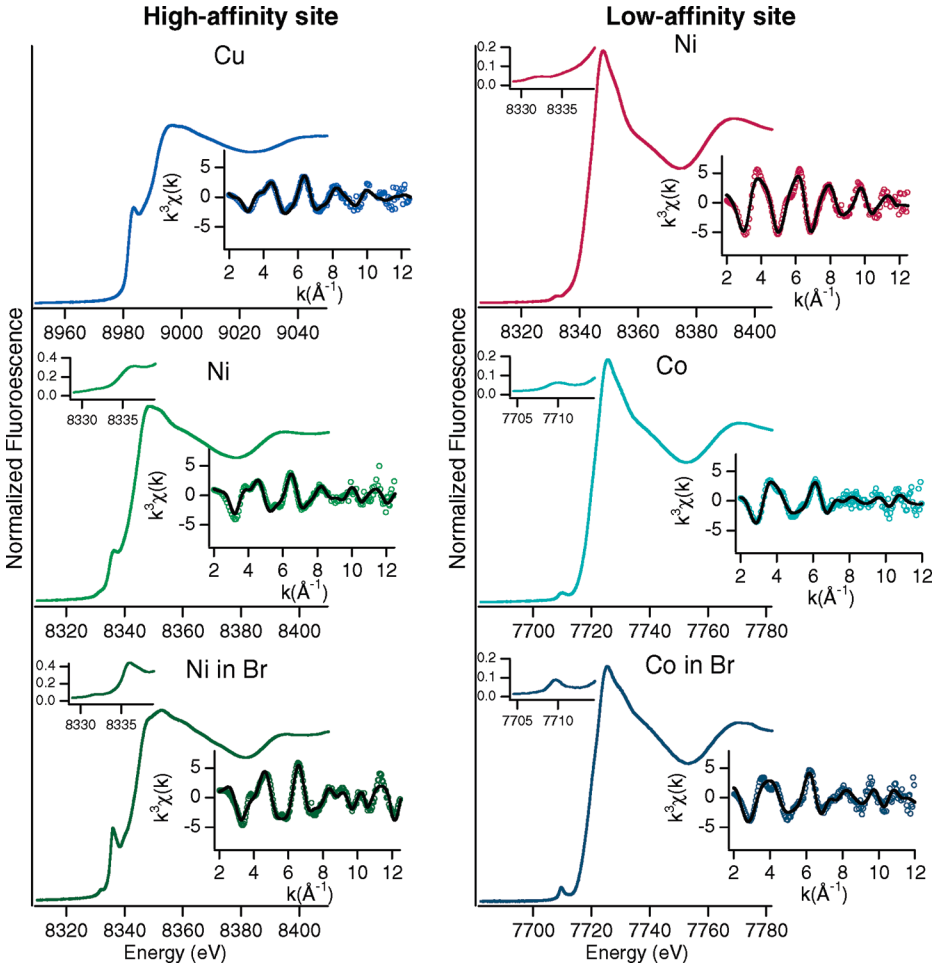

Figure 4. *K*-edge XANES and unfiltered EXAFS spectra (circles) and fits (lines) for bimetallic NikR complexes, CuNi−NikR and NiCo−NikR, where the first metal is in the high-affinity metal-binding site (left) and the second metal is in the low-affinity metal-binding site (right). The range of the *k*-space fit is 2−12 Å^{-1} for Co(II) and 2−12.5 Å^{-1} for Ni(II) and Cu(II).

residues available and none near where the putative low-affinity site is proposed on the basis of the *P. horikoshii* structure.[4] However, sulfur-donor and chloride ligands cannot be distinguished by EXAFS analysis, allowing for the possibility that the apparent S-donor in the fits is really a chloride ligand derived from the buffer. To test this possibility, NiCo−NikR + P_{nik} was prepared replacing buffer chloride with bromide. The presence of bromide in the buffer results in a marked change in the Co XANES spectrum, as shown in Figure 5A. The 1s → 3d peak area increases in intensity (area = 0.143(3) Å) which is more consistent with a five-coordinate complex than with a six-coordinate complex. The change in coordination is consistent with the UV−vis (Figure 5B) data, where much stronger d−d transitions are seen in the presence of bromide. EXAFS confirms that bromide is not incorporated into the Co(II) complex but rather leads to a lower coordination number from the loss of the Cl^- ligand. The remaining ligands fit very similarly to the Co(II) low-affinity site in the chloride complex: two histidine ligands at an average Co−N distance of 1.93(3) Å and three N/O-donors at an average distance of 2.08(3) Å, 0.05 Å shorter than in the chloride complex.

Effects of the Low-Affinity Site on the High-Affinity Site. The XANES of the high-affinity site metals in the bimetallic NikR complexes reveals subtle differences from the corresponding high-affinity site metals in complexes where the low-affinity sites are vacant. The changes suggest that some degree of communication exists between the high-affinity and low-affinity sites. The high-affinity Ni(II) site in NiCo−NikR loses some intensity of the 1s → 4p_z peak, signifying a decrease in the apparent planarity of the site.[50] This could result in a distortion in the planar site structure or in the presence of a mixture of complexes with different coordination numbers (e.g., four-coordinate planar + six-coordinate). The best EXAFS fits show that the ligand selection is the same as the Ni(II)−NikR protein with *ca.* two imidazole N-donors, an additional N/O-donor, and a S-donor, but one Ni−N/O distance is drastically lengthened, an increase of ∼0.4 Å in comparison to Ni(II)−NikR. Unfortunately, this effect could not be checked for the Cu(II) site in CuNi−NikR because the sample photoreduced in the X-ray beam. The reduction of the Cu(II) site was exacerbated by increased exposure if the Ni *K*-edge data was collected first. Upon exposure to X-rays, there is an increase in intensity of the pre-edge shoulder, making it difficult to form any sound conclusions about this site (see Supporting Information). Cu(II)−NikR can be made much more concentrated than bimetallic protein without any precipitation, and the amount of photoreduction over the course of this experiment for Cu(II)−NikR is insignificant.

Structural changes in the Cu(II) sites in Cu(II)−NikR and CuNi−NikR can be assessed by EPR. For Cu(II)−NikR, the

(50) Xia, J.; Lindahl, P. A. *Biochemistry* **1995**, *34*, 6037−42.

Table 2. XAS Data for Low-Affinity and High-Affinity Sites in Bimetallic NikR Complexes

NikR complex	geometry	CN[a]	*N*[b]	*r* (Å)[c]	σ^2 ($\times 10^3$Å^{-2})[d]	ΔE_0 (eV)	GOF[e]
			CuNi−NikR + P_{nik} in 20 mM TrisCl (pH 8.3), 100 mM NaCl				
Cu(II)	planar	4	2 Cu−N_{imd}	1.970(10)	7.9(7)	7.4(7)	0.56
			1 Cu−N/O	2.018(22)	[7.9][f]	[7.4]	
			1 Cu−S	2.167(16)	16.6(25)	12.5(17)	
Ni(II)	octahedral	6	2 Ni−N_{imd}	1.992(6)	3.4(5)	7.8(4)	0.82
			4 Ni−N/O	2.106(3)	[3.4]	[7.8]	
			NiCo−NikR + P_{nik} in 20 mM TrisCl (pH 8.3), 100 mM NaCl				
Ni(II)	planar	4	2 Ni−N_{imd}	1.938(5)	4.6(6)	11.6(6)	0.62
			1 Ni−N/O	2.321(16)	[4.6]	[11.6]	
			1 Ni−S	2.190(5)	2.8(5)	−4.7(15)	
Co(II)	octahedral	6	2 Co−N_{imd}	1.931(11)	5.6(1)	−5.7(12)	0.78
			3 Co−N/O	2.141(28)	[5.6]	[−5.7]	
			1 Co−S	2.216(20)	6.7(4)	−13.4(39)	
			4 Co−C_{imd}	3.122(15)	7.8(2)	15.1(11)	
			NiCo−NikR + P_{nik} in 20 mM TrisBr (pH 8.3), 100 mM NaBr				
Ni(II)	planar	4	2 Ni−N_{imd}	1.884(3)	0.8(2)	9.6(5)	0.65
			1 Ni−N/O	2.100(23)	[0.8]	[9.6]	
			1 Ni−S	2.155(5)	2.4(1)	7.0(13)	
			4 Co−C_{imd}	3.081(12)	3.8(9)	0.6(14)	
Co(II)	trigonal bipyrimadal	5	2 Co−N_{imd}	1.926(8)	2.7(6)	−3.0(9)	0.94
			3 Co−N/O	2.084(7)	[2.7]	[−3.0]	
			4 Co−C_{imd}	3.081(12)	3.8(9)	0.6(14)	

[a] CN is the overall coordination number. [b] *N* is the number of bonds at a specific distance. [c] *r* (Å) is the bond distance. [d] σ^2 is the mean square disorder in the Ni−X distance, where X is the scattering atom. [e] GOF (goodness of fit) was calculated as described in the Experimental Section. The accuracy of distance determined by EXAFS for atoms in the first coordination sphere of the metal is limited to ±0.02 Å by the theoretical phase parameters; numbers in parentheses represent standard deviations from the least-squares fits. [f] Values of parameters in [] were constrained to be equal to those of other scattering atoms in the same shell.

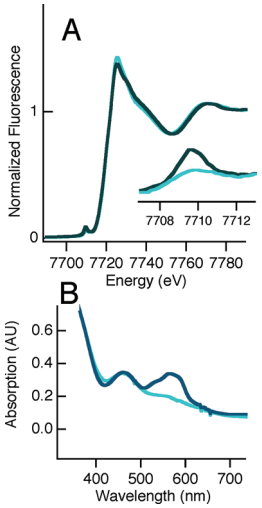

Figure 5. (A.) Co *K*-edge XANES spectra of NiCo−NikR in 20 mM TrisCl buffer with 100 mM NaCl, pH = 8.3 (light teal) and in 20 mM TrisBr with 100 mM NaBr, pH 8.3 (navy). Inset: Enlargement of the region containing the 1s → 3d transition. (B.) Electronic absorption spectra of NiCo−NikR in 20 mM TrisCl with 100 mM NaCl, pH 8.3 (light teal) and in 20 mM TrisBr with 100 mM NaBr, pH 8.3 (navy). Each spectrum is normalized to 1 mM Co. P_{nik} concentration in each case is 0.55 mM.

spectrum is characterized by $g_{||} = 2.17$, $g_{\perp} = 2.05$, and $A_{||} = 201 \times 10^{-4}$ cm^{-1}. In the CuNi−NikR, the parameters are $g_{||} = 2.17$, $g_{\perp} = 2.07$, and $A_{||} = 212 \times 10^{-4}$ cm^{-1}. These results are consistent with a very small perturbation on the Cu(II) site when Ni(II) is present in the low-affinity site (see Supporting Information). Larger values of $A_{||}$ and smaller values of $g_{||}$ are characteristic of four-coordinate planar complexes, which have a strong in-plane ligand field. Examples include a Cu(II)−tetraphenylporphyrin, where $A_{||} = 206 \times 10^{-4}$ cm^{-1} and $g_{||} = 2.19$, and Cu(II)−phthalocyanine, where $A_{||} = 217 \times 10^{-4}$ cm^{-1} and $g_{||} = 2.16$.[51,52]

Discussion

The results of the P_{nik}-lacZ reporter assay establish that in *E. coli*, NikR-dependent transcriptional repression of the *nikABCDE* operon is nickel-specific. A geometry-induced metal-specific response in metalloregulatory proteins is emerging as a theme in transcriptional regulation. The varying protein conformations exhibited by different metal complexes of these proteins offer an explanation as to how these proteins with extremely high K_d's for a variety of transition-metal ions are able to discriminate between metals *in vivo*. In a study by Pennella *et al.*, *Staphylococcus aureus* CzrA and *Mycobacterium tuberculosis* NmtR were each substituted with Zn(II), Co(II), and Ni(II).[23] CzrA is a Co(II)/Zn(II) responsive regulator that regulates expression of a Co(II)/Zn(II) facilitated pump. NmtR is responsible for the *nmt* operon, which encodes a P-type ATPase metal efflux pump, NmtA. It was found that in CzrA, the protein was only active when Zn(II) or Co(II), which binds in tetrahedral geometries, was coordinated, but Ni(II), which bound in an octahedral environment, was not active. In contrast, in NmtR, which has a similar affinity for Zn(II) and Ni(II),[53] only the octahedral Ni(II) was active. Co(II), which binds in a five- or six-coordinate ligand arrangement, was also found to be active, but only as an intermediate inducer, while Zn(II)−NmtR has no effect on derepression *in vivo*. NmtR selects for activity by having a metal center with a higher coordination environment.

Co(II)−NikR exhibited the largest change in ligand selection/geometry and was the only metal to coordinate without the cysteine thiolate ligand. For the full-length protein under

(51) Manoharan, P. T.; Rogers, M. T. *Electron Spin Resonance of Metal Complexes*; Plenum: New York, 1969; p 143.
(52) Guzy, C. M.; Raynor, J. B.; Symons, M. C. R. *J. Chem. Soc. A* **1969**, 2299−2303.
(53) Cavet, J. S.; Meng, W. M.; Pennella, M. A.; Applehoff, R. J.; Giedroc, D. P.; Robinson, N. J. *J. Biol. Chem.* **2002**, *277*, 38441−38448.

conditions involved in this study, the Co(II) complex formed with the high-affinity NikR site is clearly six-coordinate and lacks a S-donor ligand. This is consistent with UV−vis data, which do not show any intense absorptions in the near-IR region that are associated with tetrahedral Co(II) sites (see Supporting Information).[54] This site differs from the four- or five-coordinate planar or pyramidal geometries identified previously in the Co(II)−NikR complex using UV−vis spectroscopy alone.[22]

The metal ion-substituted NikR proteins show a range of metal geometries and ligand environments that result in a unique structure for each metal site. The cognate metal, Ni(II), and the Zn(II) and Cu(II) complexes all form four-coordinate complexes with $(N/O)_3S$ ligand donor that involve at least two histidine imidazole ligands. However, the geometries are distinct: Zn adopts a tetrahedral geometry, whereas Cu(II) and Ni(II) are planar. The four-coordinate Cu(II) complex shows a distinct distortion involving the lengthening of the M−S bond and one $M-N_{his}$ bond, which distinguishes it from the Ni(II) complex. Since Cu(II) is unlikely to be encountered in the reducing environment of the cell, perhaps the more biologically relevant Cu complex is that formed with Cu(I).[55,56] The Cu(I) complex is clearly distinct from Ni(II)−NikR and other metal complexes, since it is best described as a three-coordinate complex with $(N/O)_2S$ ligation, involving coordination of at least one histidine imidazole. This coordination might arise from loss of the H76′ ligand upon reduction. This His ligand is derived from the α3 helix of a second subunit and is not always resolved in the crystal structures of apo-NikR.[16,20] If this model is correct, it points to an allosteric mechanism since Ni(II) is able to induce the proper allosteric response to lock this helix into the proper place for donation of H76′ to the metal, while Cu(I) would give rise to a different allosteric response involving the α3 helix.

One possible connection between the structural flexibility and the nickel-specific response is that the coordination geometry and ligand selection observed for each metal results in a unique protein conformation or equilibrium mixture of conformations. Such a mechanism would require that the protein be able to sample many conformations. This appears to be the case for NikR. Four residues per chain are known to directly participate in Ni(II) binding,[15,16] and their backbone amide positions show very little change between the apo- and Ni(II)-bound structures.[16] However, the recent crystal structure determinations of a NikR homologue from the thermophile *P. horikoshii* show that it can adopt different conformations in the presence of varying amounts of Ni(II),[17] and the conformation of *E. coli* NikR is also dependent on DNA binding.[20] In *E. coli* NikR, a drastic conformational change is observed upon binding to DNA, as shown in a recent co-crystal structure, in comparison to apo- or holo-NikR.[16,20] These data demonstrate that the protein is quite flexible and that conformations are influenced by metal loading and the presence of DNA. Additionally, in *H. pylori* NikR, there is a Trp residue 30 Å from the high-affinity metal site that was used to probe the fluorescence response to different first-row transition metals.[18] Different degrees of Trp fluorescence quenching were observed in the presence of distinct metals, indicating variations in solvent accessibility that suggest unique conformations are present depending on the metal ion that is bound. In a protein stability study, Dias and Zamble found that *E. coli* Ni(II)−NikR was the least susceptible metal complex to proteolytic cleavage and that Cu(II) was nearly as stable as Ni(II),[57] although Ni(II)−NikR is clearly the most stable from guanidinium denaturation studies.[22] The high-affinity site structural information found for NikR complexes is consistent with the results of these studies.

The metal-induced conformational changes likely extend beyond the metal-binding residues leading to different H/D exchange for amide protons as a function of metal ion bound. Ni(II)−NikR produced the greatest difference in H/D exchange relative to apo-NikR protein. At all time points, Cu(II)−NikR exhibited less of a difference in H/D exchange. Zn(II)− and Co(II)−NikR are either not different from apo-NikR or even appear to have slightly greater exchange of amide protons on the 5−10 min time scale. While the exchange data correlate with the XAS analysis of M(II)-binding geometry, these different effects suggest that random M(II)-binding does not account for the difference in H/D exchange seen with Ni(II)−NikR relative to apo-NikR. Rather, it is the capability of Ni(II), and to a lesser extent Cu(II), to propagate conformational changes beyond the metal-binding sites. These are the only two metals found to bind in a four-coordinate planar geometry and use similar, if not identical, ligands. The crystallographic studies of the structure of *E. coli* NikR reveals that in three of the four subunits the α3 helix (residues 60−82) is disordered in the apo-NikR structure[16] but becomes ordered upon Ni(II) binding to the high-affinity site.[20] Different ligand selections or metal site geometries at the high-affinity site may lead to a different conformation in this region and thus to varying degrees of H/D exchange. In either case, the metals evoke a specific response from the protein, the degree of which is reflected by the H/D exchange studies.

Implicit in a metal-specific protein conformational response hypothesis is that protein conformation influences DNA affinity. In the case of NikR, binding to DNA involves a dyad symmetric binding site and widely separated N-terminal domains.[2] Bloom and Zamble have shown that the binding affinities of Ni(II)−NikR and Cu(II)−NikR both have nanomolar affinity for P_{nik}, however, the binding affinity for other M(II)−NikR complexes is reduced.[14] For Zn(II)−NikR, the change from a four-coordinate planar complex to a tetrahedral one is associated with the reduction of the affinity for DNA in the Zn(II) complex by 100-fold.[14] The possible structural explanations would include a protein conformation that is unable to interact strongly with both halves of the dyad symmetric DNA binding site.

Tight binding of *E. coli* NikR to DNA is associated with occupancy of the low-affinity metal sites.[2,14] The XAS studies of bimetallic NikR complexes provide some of the first detailed information regarding these sites. Both the CuNi−NikR sample and the NiCo−NikR sample feature metal sites with stoichiometry of one-half that of the high-affinity site metal (Ni(II) and Co(II), respectively), as expected from the crystal structures of *P. horikoshii* NikR.[4] While the series of structures determined give a reasonable understanding of protein conformations available, the structure of the low-affinity binding site is poorly determined and the geometry at the site is not well-defined. There are two structures that model low-affinity site coordination. In the crystal structure in the absence of PO_4^{3-}, there are

(54) Cotton, F. A. *Chemical Applications of Group Theory*, 3rd ed.; John Wiley & Sons: New York, 1990.
(55) Rosenzweig, A. C. *Acc. Chem. Res.* **2001**, *34* (2), 119−128.
(56) Finney, L. A.; O'Halloran, T. V. *Science* **2003**, *300*, 931−6.
(57) Dias, A. V.; Zamble, D. B. *J. Biol. Inorg. Chem.* **2005**, *10*, 605−612.

only three O-donors within 3 Å of the low-affinity Ni(II) ion and the geometry is consistent with incomplete formation of this site. In the second crystal structure in the presence of PO_4^{3-}, the site gains a more likely six-coordinate structure, coordinated entirely by O-donors with distances varying from 2.2 to 3.2 Å, and the site geometry is not well-resolved. Recently, a structure of *E. coli* NikR bound to a 30-bp fragment of DNA including the P_{nik} operator sequence was published.[20] In this case, the putative low-affinity binding sites contain a K^+ ion that is ligated by two conserved side chains from E30 and D34, the latter binding in a bidentate fashion. Additionally, there are three backbone O-donors from I116, Q118, and V121. The ligand with the smallest bond distance is backbone O-donor of I116 at 2.38 Å from the metal center. While the crystallography provides an insight into which residues provide the N/O donors, the XAS structure is needed to get a better indication of geometry and coordination environment of the low-affinity site. The samples studied here were all DNA complexes because it was found that loading more metals in the absence of DNA than required to fill the high-affinity sites leads to precipitation of the protein. This might arise if the low-affinity sites were poorly formed in the absence of DNA, as suggested by the crystal structures, leading to nonspecific and deleterious binding of metal ions.

The effects of occupying the low-affinity metal site on the structure of the high-affinity site are significant. The structure of the high-affinity site in the bimetallic DNA complexes is four-coordinate and planar with the same ligand environment as found for the high-affinity site in the absence of low-affinity site metals and DNA.[15] In no case involving a sample with the low-affinity sites occupied have we observed a change from four- to six-coordinate accompanied by loss of the Cys ligand that was observed for the high-affinity site in the absence of low-affinity site metals.[15] However, a six-coordinate structure consistent with the earlier XAS data has been reported in *H. pylori* NikR, again in the absence of low-affinity site metals and DNA.[19] Analysis of XAS data from the high-affinity sites shows subtle changes in the four-coordinate planar structure when the low-affinity metal sites are occupied. These changes enhance the features associated with the planar structure and suggest that the planar high-affinity site is reinforced by occupancy of the low-affinity metal site, perhaps by eliminating other conformations of the protein that introduce disorder in the high-affinity site structure.

Acknowledgment. This work was supported by the National Institutes of Health Grant GM69696 (M. J. M.), an NIH National Research Service Award T32 GM08515 (S. L.), and National Science Foundation Grant MCB0520877 (P. T. C.). XAS data collection at the National Synchrotron Light Source at Brookhaven National Laboratory was supported by the U.S. Department of Energy, Division of Materials Sciences and Division of Chemical Sciences. Beamline X9B at NSLS is supported in part by the NIH. Portions of this research were carried out at the Stanford Synchrotron Radiation Laboratory, a national user facility operated by Stanford University on behalf of the U.S. Department of Energy, Office of Basic Energy Sciences. The SSRL Structural and Molecular Biology Program is supported by the Department of Energy, Office of Biological and Environmental Research, and by the National Institutes of Health, National Center for Research Resources, Biomedical Technology Program. Mass spectrometry data were collected at the Washington University Center for Biomedical and Bioorganic Mass Spectrometry, a National Institutes of Health National Center for Research Resources (Grant No. P41RR0954). P. T. C. and M. J. B. thank David Hambly, Justin Sperry, and Dr. Michael Gross for assistance with the mass spectrometry experiments.

Supporting Information Available: Tables for XAS data for Fourier-filtered analyses of NikR proteins. XANES spectra of CuNi−NikR showing photoreduction in the X-ray beam. EPR spectra of Cu(II)−NikR and CuNi−NikR. LC-ESI-MS spectra of H/D exchange samples. This material is available free of charge via the Internet at http://pubs.acs.org.

JA068505Y